Biomedical Optics EXPRESS

Imaging granularity of leukocytes with third harmonic generation microscopy

Cheng-Kun Tsai,[1] Yu-Shing Chen,[1] Pei-Chun Wu,[1] Tsung-Yuan Hsieh,[1] Han-Wen Liu,[1] Chiou-Yueh Yeh,[2] Win-Li Lin,[1] Jean-San Chia,[2] and Tzu-Ming Liu[1,3,*]

[1]*Institute of Biomedical Engineering, National Taiwan University, No. 1, Sec. 4, Roosevelt Road, Taipei 10617, Taiwan*

[2]*Graduate Institute of immunology, College of Medicine, National Taiwan University, No. 1, Jen-Ai Road, Taipei 10048, Taiwan*

[3]*Molecular Imaging Center, National Taiwan University, No. 1, Sec. 4, Roosevelt Road, Taipei 10617, Taiwan*

**tmliu@ntu.edu.tw*

Abstract: Using third harmonic generation (THG) microscopy, we demonstrate that granularity differences of leukocytes can be revealed without a label. Excited by a 1230 nm femtosecond laser, THG signals were generated at a significantly higher level in neutrophils than other mononuclear cells, whereas signals in agranular lymphocytes were one order of magnitude smaller. Interestingly, the characteristic THG features can also be observed *in vivo* to track the newly recruited leukocytes following lipopolysaccharide (LPS) challenge. These results suggest that label-free THG imaging may provide timely tracking of leukocyte movement without disturbing the normal cellular or physiological status.

OCIS codes: (180.4315) Nonlinear microscopy; (170.1530) Cell analysis.

References and links

1. R. N. Germain, M. J. Miller, M. L. Dustin, and M. C. Nussenzweig, "Dynamic imaging of the immune system: progress, pitfalls and promise," Nat. Rev. Immunol. **6**(7), 497–507 (2006).
2. A. P. Cairns, A. D. Crockard, J. R. McConnell, P. A. Courtney, and A. L. Bell, "Reduced expression of CD44 on monocytes and neutrophils in systemic lupus erythematosus: relations with apoptotic neutrophils and disease activity," Ann. Rheum. Dis. **60**(10), 950–955 (2001).
3. M. Rajadhyaksha, S. González, J. M. Zavislan, R. R. Anderson, and R. H. Webb, "In vivo confocal scanning laser microscopy of human skin II: advances in instrumentation and comparison with histology," J. Invest. Dermatol. **113**(3), 293–303 (1999).
4. S. González, R. Sackstein, R. R. Anderson, and M. Rajadhyaksha, "Real-time evidence of in vivo leukocyte trafficking in human skin by reflectance confocal microscopy," J. Invest. Dermatol. **117**(2), 384–386 (2001).
5. C. Li, R. K. Pastila, C. Pitsillides, J. M. Runnels, M. Puoris'haag, D. Côté, and C. P. Lin, "Imaging leukocyte trafficking in vivo with two-photon-excited endogenous tryptophan fluorescence," Opt. Express **18**(2), 988–999 (2010).
6. R. S. Lim, J. L. Suhalim, S. Miyazaki-Anzai, M. Miyazaki, M. Levi, E. O. Potma, and B. J. Tromberg, "Identification of cholesterol crystals in plaques of atherosclerotic mice using hyperspectral CARS imaging," J. Lipid Res. **52**(12), 2177–2186 (2011).
7. M. Rehberg, F. Krombach, U. Pohl, and S. Dietzel, "Label-free 3D visualization of cellular and tissue structures in intact muscle with second and third harmonic generation microscopy," PLoS ONE **6**(11), e28237 (2011).
8. L. Liu, J. A. Gardecki, S. K. Nadkarni, J. D. Toussaint, Y. Yagi, B. E. Bouma, and G. J. Tearney, "Imaging the subcellular structure of human coronary atherosclerosis using micro-optical coherence tomography," Nat. Med. **17**(8), 1010–1014 (2011).
9. L. Golan, D. Yeheskely-Hayon, L. Minai, E. J. Dann, and D. Yelin, "Noninvasive imaging of flowing blood cells using label-free spectrally encoded flow cytometry," Biomed. Opt. Express **3**(6), 1455–1464 (2012).
10. C.-K. Sun, S.-W. Chu, S.-Y. Chen, T.-H. Tsai, T.-M. Liu, C.-Y. Lin, and H.-J. Tsai, "Higher harmonic generation microscopy for developmental biology," J. Struct. Biol. **147**(1), 19–30 (2004).
11. N. Olivier, M. A. Luengo-Oroz, L. Duloquin, E. Faure, T. Savy, I. Veilleux, X. Solinas, D. Débarre, P. Bourgine, A. Santos, N. Peyriéras, and E. Beaurepaire, "Cell lineage reconstruction of early zebrafish embryos using label-free nonlinear microscopy," Science **329**(5994), 967–971 (2010).
12. S.-Y. Chen, H.-Y. Wu, and C.-K. Sun, "In vivo harmonic generation biopsy of human skin," J. Biomed. Opt. **14**(6), 060505 (2009).

#171483 - $15.00 USD Received 27 Jun 2012; revised 6 Aug 2012; accepted 7 Aug 2012; published 24 Aug 2012

13. S.-Y. Chen, S.-U. Chen, H.-Y. Wu, W.-J. Lee, Y.-H. Liao, and C.-K. Sun, "In vivo virtual biopsy of human skin by using noninvasive higher harmonic generation microscopy," IEEE J. Sel. Top. Quantum Electron. **16**(3), 478–492 (2010).
14. M.-R. Tsai, S.-Y. Chen, D.-B. Shieh, P.-J. Lou, and C.-K. Sun, "In vivo optical virtual biopsy of human oral mucosa with harmonic generation microscopy," Biomed. Opt. Express **2**(8), 2317–2328 (2011).
15. D. Débarre, W. Supatto, A.-M. Pena, A. Fabre, T. Tordjmann, L. Combettes, M.-C. Schanne-Klein, and E. Beaurepaire, "Imaging lipid bodies in cells and tissues using third-harmonic generation microscopy," Nat. Methods **3**(1), 47–53 (2006).
16. R. R. Anderson, W. Farinelli, H. Laubach, D. Manstein, A. N. Yaroslavsky, J. Gubeli 3rd, K. Jordan, G. R. Neil, M. Shinn, W. Chandler, G. P. Williams, S. V. Benson, D. R. Douglas, and H. F. Dylla, "Selective photothermolysis of lipid-rich tissues: a free electron laser study," Lasers Surg. Med. **38**(10), 913–919 (2006).
17. P. Wang, H.-W. Wang, M. Sturek, and J.-X. Cheng, "Bond-selective imaging of deep tissue through the optical window between 1600 and 1850 nm," J Biophotonics **5**(1), 25–32 (2012).
18. European mutant mouse pathology database (Pathbase), "Scanning electron microscopy of the mouse ear," (University of Cambridge, 08/2009). http://eulep.pdn.cam.ac.uk/~skinbase/Anatomic_hair_types/EAR_ ANNOTAT ED.jpg.
19. C. W. Freudiger, W. Min, B. G. Saar, S. Lu, G. R. Holtom, C. He, J. C. Tsai, J. X. Kang, and X. S. Xie, "Label-free biomedical imaging with high sensitivity by stimulated Raman scattering microscopy," Science **322**(5909), 1857–1861 (2008).
20. C. F. Chang, C. H. Yu, and C.-K. Sun, "Multi-photon resonance enhancement of third harmonic generation in human oxyhemoglobin and deoxyhemoglobin," J Biophotonics **3**(10-11), 678–685 (2010).
21. M. H. Abdulreda, G. Faleo, R. D. Molano, M. Lopez-Cabezas, J. Molina, Y. Tan, O. A. Echeverria, E. Zahr-Akrawi, R. Rodriguez-Diaz, P. K. Edlund, I. Leibiger, A. L. Bayer, V. Perez, C. Ricordi, A. Caicedo, A. Pileggi, and P. O. Berggren, "High-resolution, noninvasive longitudinal live imaging of immune responses," Proc. Natl. Acad. Sci. U.S.A. **108**(31), 12863–12868 (2011).
22. J. Fujisaki, J. Wu, A. L. Carlson, L. Silberstein, P. Putheti, R. Larocca, W. Gao, T. I. Saito, C. L. Celso, H. Tsuyuzaki, T. Sato, D. Côté, M. Sykes, T. B. Strom, D. T. Scadden, and C. P. Lin, "In vivo imaging of Treg cells providing immune privilege to the haematopoietic stem-cell niche," Nature **474**(7350), 216–219 (2011).
23. J. Condeelis and J. W. Pollard, "Macrophages: obligate partners for tumor cell migration, invasion, and metastasis," Cell **124**(2), 263–266 (2006).
24. M.-C. Chan, T.-M. Liu, S.-P. Tai, and C.-K. Sun, "Compact fiber-delivered Cr:forsterite laser for nonlinear light microscopy," J. Biomed. Opt. **10**(5), 054006 (2005).
25. T.-M. Liu, M.-C. Chan, I.-H. Chen, S.-H. Chia, and C.-K. Sun, "Miniaturized multiphoton microscope with a 24Hz frame-rate," Opt. Express **16**(14), 10501–10506 (2008).
26. S.-H. Chia, C.-H. Yu, C.-H. Lin, N.-C. Cheng, T.-M. Liu, M.-C. Chan, I.-H. Chen, and C.-K. Sun, "Miniaturized video-rate epi-third-harmonic-generation fiber-microscope," Opt. Express **18**(16), 17382–17391 (2010).

1. Introduction

The *in vivo* study of leukocytes is challenging due to their nature of fast trafficking, multiple lineages, frequent cell-cell interactions, and dynamic activation or maturation in immune response processes. Using confocal or multiphoton fluorescence microscopy, *in vivo* dynamics and microenvironments of immune systems can be dissected at a high spatial and temporal resolution [1]. For precise analysis and correct interpretation *in vivo*, multiple color labeling is required to time-course monitor many cellular markers and signaling molecules at the same time. For this purpose, much effort is needed to develop and maintain multiple independent lines of mice expressing different color fluorescent proteins. Limited by the spectral bleed through of fluorescent proteins, the number of labeling colors is typically below four [1]. Therefore, if the lineages or types of leukocytes can be preliminarily differentiated without a label, then the types of immune cells can be identified more specifically. If specific enough, a label for lineage identification can even be saved for other parameters, and can thus increase the dimensions of analysis in image cytomics. In addition, no specific fluorescence labeling is currently approved for use in clinical diagnosis to identify human leukocytes *in vivo*. A label-free microscopy method that can show different types of leukocytes *in vivo* would be a critical first step toward the development of virtual optical biopsy of immune cells.

In conventional flow cytometry of leukocytes, it is well known that side-scattering properties can be used to categorize neutrophils (high scattering), monocytes (medium scattering), and lymphocytes (low scattering) in peripheral blood [2]. Such optical scattering originates from the lipid bodies and vesicles insides the leukocytes, which makes them appear white in the buffy coat fraction of blood centrifugation. By exploiting this scattering contrast,

#171483 - $15.00 USD Received 27 Jun 2012; revised 6 Aug 2012; accepted 7 Aug 2012; published 24 Aug 2012

reflectance confocal microscopy can recognize human leukocytes *in vivo* through their sizes and motile features [3,4]. Better three-dimensional (3D) resolution and contrast can be achieved in mouse tissues by exploiting the leukocyte's endogenous ultraviolet fluorescence of tryptophan [5] with lipid R-CH_2–R stretching modes in coherent anti-Stokes Raman scattering microscopy [6] or with label-free third harmonic generation (THG) microscopy [7]. However, these previous imaging studies mainly focused on the *in vivo* trafficking properties of leukocytes, and not their granularity or types. Only one recent report used micro-optical coherence tomography (μ-OCT) to observe the morphological differences among leukocytes *in vivo* with 1 μm spatial resolution [8]. Using spectrally encoded flow cytometry, better morphological features on leukocytes *in vivo* can be resolved with 0.7 μm transverse resolution in the lower lips of humans [9]. However, subcellular details of lipid granules should be revealed with higher 3D imaging resolution and contrast in order to identify and differentiate the leukocytes with less ambiguity and more specificity.

Third harmonic generation microscopy with excitation at around 1230 nm can noninvasively reveal cellular morphology, subcellular organelles, and melanin distributions in deep tissues for the application of developmental biology [10,11] and clinical diagnosis [12–14] without labeling. In deep tissues, this technique has less background interference than reflectance confocal microscopy and better transverse resolution (~500 nm) [14] than infrared laser-based μ-OCT and spectrally encoded confocal microscopy. The most important aspect is the fact that THG processes excited at around 1210 nm can be resonantly enhanced by lipid bodies or vesicles [15], which are abundant in leukocytes. This molecular enhancement mechanism is due to the dipolar-active second overtone of the R-CH_2–R stretching modes in lipids [16,17]. Such characteristic infrared absorption bands around 1210 nm have been used for photothermolysis of lipid-rich tissues [16], and provide strong photoacoustic contrast for lipids in deep tissues [17].

Given these advantages, we demonstrate in this study that the difference in granularity, which is an obvious phenotype of leukocytes, can be revealed by high resolution THG microscopy. The R-CH_2–R stretching modes of lipid granules can enhance the THG signals in leukocytes. Through an *in vitro* test, granular neutrophils showed much higher THG contrast than monocytes and agranular lymphocytes. These differences in THG features in leukocytes can also be observed in lipopolysaccharide (LPS) challenge sites in mouse ears *in vivo*. This approach can potentially be used in the study of immune cytomics, virtual optical biopsy on inflammation sites, or label-free flow cytometry for clinical use [9].

2. Imaging setup

To characterize leukocytes and their microenvironments, multimodal nonlinear microscopy, including two-photon fluorescence (TPF, 665-750 nm), second harmonic generation (SHG, ~615 nm), and third harmonic generation (~410 nm) were used to measure optical contrast. The nonlinear microscopy instrument was composed of a home built femtosecond Cr:forsterite laser, a scanning unit (FV300, Olympus), an upright optical microscope, a 2D translation stage, three photomultiplier tubes (PMTs), a data acquisition card, and imaging reconstruction software. The femtosecond Cr:forsterite laser was operated at around 1230 nm with a pulse width of 100 fs. The typical output power was 500 mW. The laser spectrum had a 30 nm bandwidth and its spectral power ranged from 1200 nm to 1260 nm, which covers the 1200-1220 nm absorption band of R-CH_2–R stretching overtone in lipids [17]. The laser beam was scanned by galvanometer mirrors and passed the long-pass 665 nm-edged dichroic beam splitter (FF665-Di02-25x36, Semrock). The scanned laser beam was then focused by a 60 × NA = 1.2 water immersion objective (UPLSAPO 60XW, Olympus) onto prepared leukocytes or mounted mouse ears for the generation of nonlinear optical signals. To minimize on-focus photo damage, we kept the power below 80 mW after the objective. The point-by-point generated signals of SHG and THG were both epi-collected by the same objective, reflected by the long-pass 665 nm-edged dichroic beam splitter, which was further separated by a long-

#171483 - $15.00 USD Received 27 Jun 2012; revised 6 Aug 2012; accepted 7 Aug 2012; published 24 Aug 2012

pass 490 nm-edged dichroic beam splitter filtered by 620 ± 10 nm (for SHG) and 410 ± 5 nm (for THG) band-pass filters, and detected by two PMTs. The TPF signal was transmitted through the long-pass 665 nm-edged dichroic beam splitter and detected by another PMT in the scanning unit. The 512 × 512 pixel images were reconstructed at a 1Hz frame rate by the image acquisition software. The effective pixel dwell time was approximately 3.8 μs. To improve image quality, three frames were averaged to obtain one image. The *in vivo* sectioning capability and submicron spatial resolution of this system have been described elsewhere [10].

3. Materials and experimental methods

3.1 Isolation of neutrophils and monocytes from the peripheral blood of mice

Blood from Balb/C mice was collected by orbital puncture. The population density of neutrophils and monocytes was enriched by density gradient centrifugation with HISTOPAQUE (HISTOPAQUE-1119 and HISTOPAQUE-1077, Sigma-Aldrich). The neutrophil and monocyte fractions were examined with Wright-Giemsa stain (Sigma-Aldrich) and found to have a purity above 90%.

3.2 Isolation of lymphocytes from the spleen of mice

BALB/c mice (25 to 30 g) were anesthetized with an intraperitoneal injection of a 30-40 μl mixture of Rompun and Zoletil 50 (1 ml anesthetic is composed of 0.5 ml Zoletil 50, 0.22 ml Rompun, and 0.28 ml ddH_2O). Mice were then sacrificed, and their spleens were dissected out and washed in Hank's balanced salt solution. The spleen tissue was teased and then sandwiched between frosted glass slides. A single cell suspension was prepared by passing the suspension through sterile mesh. The red blood cells (RBCs) were lysed in cold RBC lysis buffer and washed twice with RPMI media containing 10% fetal calf serum. The splenocytes were counted using a hemocytometer to determine the viability. Flow cytometry analysis of splenocytes indicated that the percentage of CD3e positive T lymphocytes was 52.7 ± 3.92%, NK1.1 positive cells was 2.9 ± 0.1%, and CD11b positive cells was 35.9 ± 3.1%. The cell morphology of splenocytes was also examined with Wright-Giemsa stain.

3.3 Animal anesthetics and LPS challenge at the ear pinna of mice

Leukocytes were recruited for *in vivo* observation with THG, SHG, and TPF microscopy by LPS challenge on the ear pinna of BALB/c mice. Inhalation anesthetics were used for LPS administration, followed by observation with nonlinear microscopy. Isoflurane was used for its effectiveness, lack of side effects, and rapid washout, especially in continuous time-course imaging with prolonged experimental observations. We kept the anesthetized mice under surveillance and observed their reflexes and vital signs (94-163 breaths/min, 325-780 beats/min, 37.5 °C) and maintained their body temperature with a small warm package during the entire procedure until recovery.

For the LPS challenge, we subcutaneously applied 5 μg of LPS into the ear pinna of the mice to monitor the progression of the immune responses. At time points of 6-hour, 2-day, 3-day, and 6-day post-LPS induction, the mice were brought to the nonlinear optical microscopy system for SHG, and THG imaging. At each time point, the mice were anesthetized and images were recorded for less than 1.5 hours.

All of the procedures of the animal experiments described above followed the animal protocols approved by the Institutional Animal Care and Use Committee, College of Medicine, National Taiwan University, under case numbers 20090277 and 20120028. Following hygiene regulations and to avoid animal infections, the mice stayed in their cages at all times, except during the experiment periods (within one day), and were taken care of by the animal center in the College of Medicine at National Taiwan University.

#171483 - $15.00 USD Received 27 Jun 2012; revised 6 Aug 2012; accepted 7 Aug 2012; published 24 Aug 2012

4. Results

4.1 In vitro THG imaging on leukocytes with different granularity

We first investigated the THG morphological pattern and contrast yield of three major types of leukocytes: neutrophils, monocytes, and lymphocytes [Figs. 1(a)-1(g)]. The former two were mostly isolated from the peripheral blood of the mice, and lymphocytes were extracted from the spleen. These images [Figs. 1(a)-1(c)] were taken at the sectioning plane with the largest cellular cross-section area. To avoid photodamage, the laser power after the objective was 70 mW. Using a spectrometer with a cooled charge-coupled device, we measured the multiphoton nonlinear optical spectrum of leukocytes under imaging [Fig. 1(h)]. It showed a narrow THG spectrum with a peak around 410 nm. Since the two-photon resonant excitation wavelength (615 nm) of a Cr:forsterite laser is far away from the soret bands of most endogenous pigments such as reduced nicotinamide adenine dinucleotide (NADH), flavins, and porphyrins, no obvious autofluorescence was observed in the spectrum. To fairly compare THG contrast among different types of leukocytes, we excited all cells at the same mounting geometry and laser excitation intensity. In the peripheral blood fraction of neutrophils, 90% of inspected leukocytes typically had strong THG contrast throughout the cells [Fig. 1(a)] due to the densely packed lipid granules inside. Two-dimensional intensity analysis [Fig. 1(d)] and cross sectional THG profiles [Fig. 1(g), red curve] showed a saturated plateau with 8 μm diameter. In the monocyte fractions, intracellular granules with THG contrast were less densely distributed, and the average THG intensity within these cells was typically one-third of that in neutrophils [Figs. 1(b), 1(e)]. In splenocyte extracts, flow cytometry analysis showed that 50% of leukocytes had the mouse T lymphocyte-specific CD3ε marker. In a typical THG image of splenocyte extract without labeling, we found 70% of them have a feature of a hollow core [Fig. 2(a), indicated by white arrows]. Some of them have a few granules inside the cells. In contrast, other cells had more granules and higher THG signal levels within them. To confirm the THG morphology of T lymphocytes, we further immunolabeled splenocyte extracts with anti-CD3ε-Allophycocyanin (APC), which targets the specific surface CD3ε marker of mouse T lymphocytes. Leukocytes from spleen extracts were stained with APC-labeled anti-CD3 antibodies (clone 145-2C11) for 30 min and then washed with 1 × PBS buffer for THG microscopy (137 mM NaCl, 2.7 mM KCl, 10 mM Na_2HPO_4, 2 mM KH_2PO_4, pH = 7.4). The two-photon fluorescence of APC centered at 656 nm falls in the detection window of TPF contrast in our nonlinear microscopy system. For the convenience of observation with the nonlinear optical microscope, labeled cells were mounted between a cover glass and a slide with ~6 μm space in between. To avoid interference from strong interface THG, we typically acquired the sectioning images 2~3 μm away from the water-glass interface. Since TPF microscopy has poorer axial resolution than THG microscopy, in our imaging geometry, TPF signals from the membrane surfaces could still be excited and collected. Therefore, instead of a ring structure, the TPF signals from labeling dye distributed over the cross-section of cells [Figs. 2(b)-2(d)]. The corresponding THG morphology showed a hollow-core spherical shape [Figs. 1(c), 1(f), 2(c)]. As a result, the average THG intensities in T lymphocytes [Fig. 1 (g), black curve] were one order of magnitude lower than those of neutrophils [Fig. 1(g), red curve]. Compared with the bright-field image of lymphocytes [Fig. 2(e)], this observation might be due to the fact that the nuclei of lymphocytes (stained with magenta color) occupy most of the volume of whole cells. In this labeled extract, some hollow-core cells did not have anti-CD3ε-APC staining [Fig. 2(f)]. These cells might represent other lymphoid cells, such as B lymphocytes or natural killer cells. With prior knowledge on the types of leukocytes, these results indicate that leukocytes with different granularities have different morphologies and contrasts in THG microscopy. Neutrophils have extraordinarily high THG contrast that can be easily distinguished from other leukocyte populations. Lymphoid cells, due to their large single nucleus, have common features of hollow cores and stronger THG contrast at cellular boundaries.

#171483 - $15.00 USD Received 27 Jun 2012; revised 6 Aug 2012; accepted 7 Aug 2012; published 24 Aug 2012

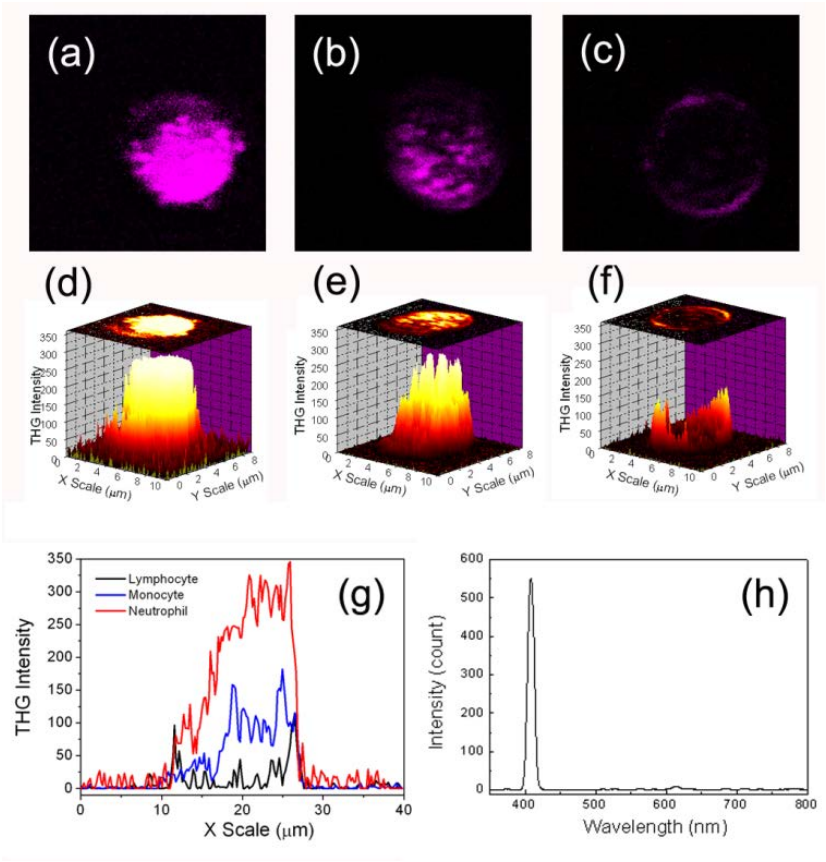

Fig. 1. Third harmonic generation images (a-c) and 3D surface plots (d-f) of a (a,d) neutrophil, (b,e) monocyte, and (c,f) lymphocyte. Field of view: 12 × 12 μm. (g) Cross sectional view of neutrophil (red curve), monocyte (blue curve), and lymphocyte (black curve). (h) Multiphoton nonlinear optical spectrum of leukocytes under imaging.

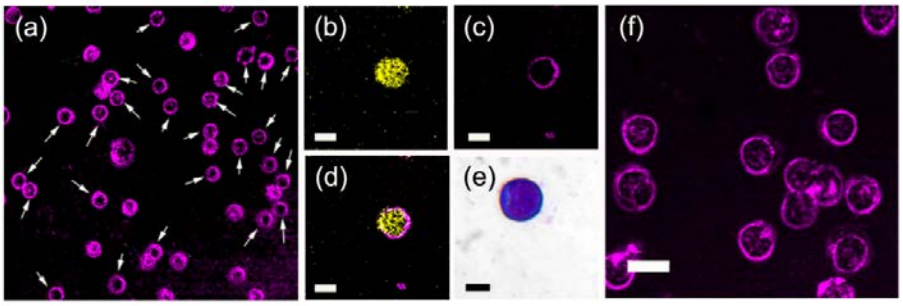

Fig. 2. (a) THG images of spleen extract. White arrows indicate hollow-core splenocytes. (b-d) The (b) TPF, (c) THG, and (d) combined images of an anti-D3ε-Allophycocyanin labeled T-lymphocyte. Scale bar: 5 μm. (e) The bright-field image of lymphocyte with Wright-Giemsa stain. Scale bar: 5 μm (f) The THG images of hollow-core leukocytes without anti-CD3ε-APC targeting in spleen extracts. Scale bar: 10 μm.

4.2 Imaging leukocytes in the context of LPS challenge

We then performed *in vivo* nonlinear microscopy on the microenvironment of a typical immune response (LPS challenge) in order to see whether the leukocytes still show these morphological differences when they enter tissues from the bloodstream. To acquire deep

#171483 - $15.00 USD Received 27 Jun 2012; revised 6 Aug 2012; accepted 7 Aug 2012; published 24 Aug 2012

tissue images, the laser power we used was 80 mW. Similar to the role differential interference contrast microscopy plays in bright-field *in vitro* microscopy, nonlinear microscopy provides 3D *in vivo* structural and morphological information to complement the fluorescence imaging. The SHG modality can image the structure of collagen networks in subcutaneous microenvironments (Fig. 3, green color). On the other hand, many resident cells in the subcutaneous microenvironment can be simultaneously visualized by THG microscopy without labeling (Fig. 3, magenta color).

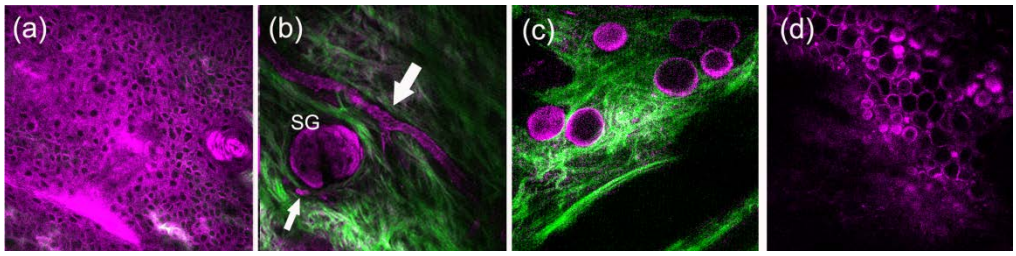

Fig. 3. Combined second harmonic generation (green color) and third harmonic generation (magenta color) images of subcutaneous microenvironments. Resident cells include (a) epitheial keratenocytes, (b) sebocytes in sebaceous gland (SG), (c) adipocytes, and (d) chondrocytes. White arrows indicate the vessels around the sebaceous gland. Field of view: 240 × 240 μm.

Compared with typical histology [18] and stimulated Raman scattering microscopy images [19] of cells from mouse ears, at different penetration depths z of ear pinna, THG microscopy can typically image epithelial keratinocytes [z = 0, Fig. 3(a)], sebocytes in sebaceous glands (SG) [z = 20-50 μm, Fig. 3(b)], adipocytes around deep vessels [z = 80-120 μm, Fig. 3(c)], and densely packed chondrocytes in cartilage [z = 140-200 μm, Fig. 3(d)]. The vessel networks can also be observed by THG microscopy without labeling [indicated by white arrows in Fig. 3(b)]. It was resulted from a streak THG image of fast moving red blood cells, whose hemoglobin can give strong THG contrast [20]. The individual blood cells can be clearly observed using a fast (30 Hz) imaging frame rate [14]. Six hours post-LPS challenge, leukocytes with bright and saturated THG contrast started to infiltrate the tissue [Fig. 4(a)]. The bright THG contrast is the characteristic feature of neutrophils in peripheral blood. They are the first line of defense in innate immune responses and are most abundant in peripheral blood. Two other neutrophil-like cells (indicated by white arrows) adhered to the vessel wall [Fig. 4(a)], outlined by yellow dashed line] with deformed shapes, which might undergo an extravasation process. Amoeboid movement of neutrophils can also be captured *in vivo* (Fig. 5). By the second day post-LPS administration in the same mouse, the number of infiltrated neutrophil-like cells drastically increased, and hollow-core leukocytes started to appear in challenge sites. By the third day post-LPS administration, many more hollow-core leukocytes [white arrows, Figs. 4(b), 4(c)] appeared in the microenvironment. At different sectioning planes, we found elongated [Figs. 4(e), 4(f)] and ruffled leukocytes [Fig. 4(g)], which are important features for functional and motility analyses [21]. Cell-cell contact events between leukocytes with different granularities can also be observed [Fig. 4(h)]. The inflammation obviously calmed down after the fourth day. Only immobile debris or pus was left in the tissues afterwards [Fig. 4(d)].

#171483 - $15.00 USD Received 27 Jun 2012; revised 6 Aug 2012; accepted 7 Aug 2012; published 24 Aug 2012

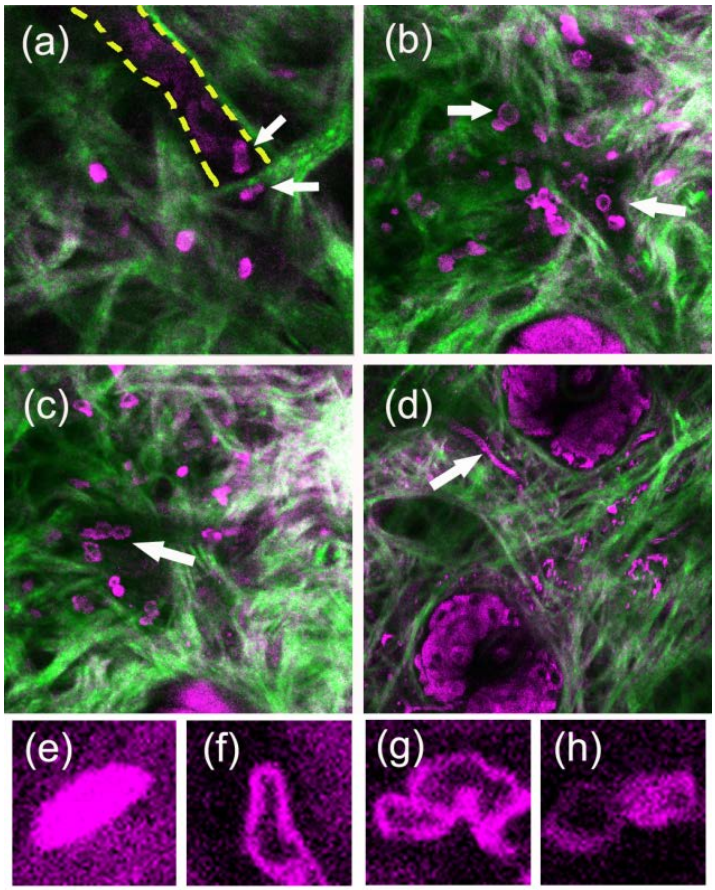

Fig. 4. Combined second harmonic generation (green color) and third harmonic generation (magenta color) time course images of inflammation microenvironments (a) 6 hours, (b),(c) 3 days, and (d) 6 days post-LPS challenge in the same mouse. White arrows indicate (a) deformed neutrophils, (b) hollow-core lymphoid cells, (c) deformed lymphoid cells, and (d) a vessel with circulating red blood cells. Bottom rows shows THG images of elongated (e) neutrophil and (f) lymphoid leukocytes, (g) ruffled lymphoid leukocytes, and (h) cell-cell contact between granulocytes and lymphoid cells. Fields of view are 120 × 120 μm in (a-d) and 12 × 12 μm in (e-h).

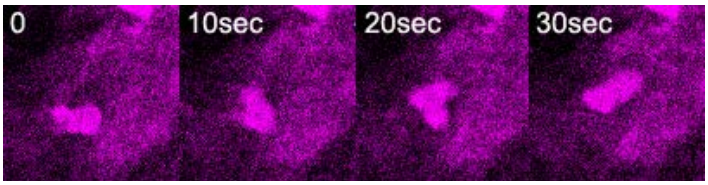

Fig. 5. Amoeboid movement of neutrophils at 3 days post-LPS challenge in Balb/c mice. Field of view: 24 × 24 μm.

To demonstrate how cell/stage statistics can be tracked in this platform, we differentiated cell types in the microenvironment of LPS challenge according to the THG features that we observed *in vitro*. Since monocytes will become macrophages when they enter tissues, we focus on the neutrophil-like (N) and lymphocyte-like (L) cells *in vivo* (Fig. 6). At time points of 10hours, 36hours, and 60hours post LPS challenge, the ICR mouse was analyzed by *in vivo* THG microscopy using the harmonic generation microscopy system. At each time point, we searched for three different places with leukocyte infiltration in mouse ear pinna. We then

#171483 - $15.00 USD Received 27 Jun 2012; revised 6 Aug 2012; accepted 7 Aug 2012; published 24 Aug 2012

took a stack of 3D sectioning on that site to acquire leukocyte morphology and distributions in three dimensions. Using the THG generated from surrounding collagen, we normalized the average THG intensity of leukocytes over them. By assessing the average intensity levels within cells and the cross sectional intensity profiles, we counted the numbers of neutrophil-like and lymphocyte-like cells. According to the statistical results, the collagen-normalized THG of neutrophil-like cells ranged from 1.44 to 1.8, which somewhat depended on the intensity of THG signals from collagen. The collagen-normalized THG of lymphocyte-like cells (from 0.75 to 1.2) was significantly lower than neutrophil-like cells. The THG contrast between neutrophil-like and lymphocyte-like cells was not as large as the *in vitro* results, which might be due to better refractive index matching with extracellular matrices or the background interference from collagen. From 10hours to 60hours post LPS administration, the density of infiltrated cells at LPS sites increased three fold.

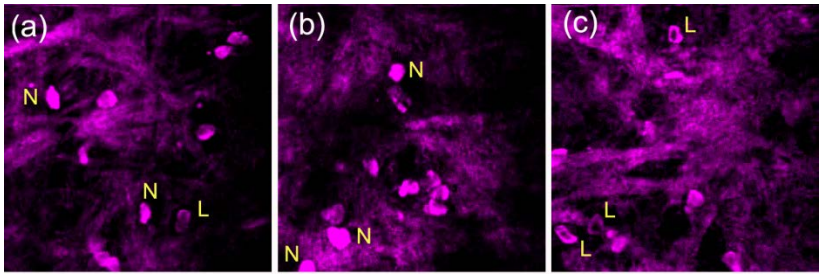

Fig. 6. *In vivo* THG images of leukocyte infiltration in an ICR mouse at (a) 10hours, (b) 36hours, and (c) 60hours post-LPS challenge in ear pinna. Neutrophils (N) and lymphoid cells (L) can be identified in the microenvironment of an immune response. THG signals around leukocytes were generated from collagen, which serves as an *in vivo* reference for the normalization of THG signals from different images.

After counting more than 30 cells, the population percentages of neutrophil-like and lymphocyte-like cells were calculated. According to the statistical results, the population percentage of neutrophil-like leukocytes in the ICR mouse increased from 13% to 20% (Fig. 7) with the progression of an immune response. Lymphocyte-like leukocytes also increased from 5.15 to 12%, though less than neutrophil-like cells.

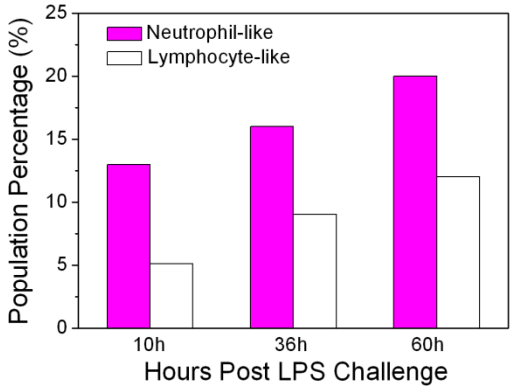

Fig. 7. Population percentages of neutrophil-like (magenta color bar) and lymphocyte-like (white color bar) leukocytes at 10hours, 36hours, and 60hours post-LPS challenge.

There was clearly a higher number of neutrophil-like leukocytes than lymphocyte-like cells, which is in agreement with the fact that neutrophils are the most abundant leukocytes in peripheral blood during first-line innate immune responses. This statistical result demonstrates that our platform of THG microscopy can be used to preliminarily evaluate the immune

#171483 - $15.00 USD Received 27 Jun 2012; revised 6 Aug 2012; accepted 7 Aug 2012; published 24 Aug 2012

dynamics of different types of leukocytes. However, labeling is still required to identify specific cell identities.

5. Discussion and conclusion

For *in vivo* microscopy, harmonic generation contrasts, such as SHG and THG, are usually considered to be modalities without molecular specificity. However, here we demonstrated that they provide a basic and useful framework through which spatial contexts, such as the distance to vessels, collagen morphologies, and interaction with resident cells can be monitored and measured in microenvironments. Employing harmonic generation contrast together with multiphoton fluorescence microscopy can provide more information for the study of complex immune responses among different types of leukocytes. We also showed that THG microscopy is sensitive to the granularity differences among leukocytes. The contrast originates from the lipid bodies or vesicles inside the granule-rich leukocytes. Through *in vitro* experiments, we found that high granularity neutrophils have extraordinarily strong THG contrast compared to agranular lymphocytes, indicating a potential index to preliminarily classify the lineage of leukocytes. In addition, using *in vivo* THG microscopy, we can determine when and where neutrophil-like and lymphocyte-like leukocytes are recruited in the microenvironments of the LPS challenge. Their sizes, morphologies, trafficking properties, and the cell-cell relationships can all be time-course recorded. These results suggest that label-free THG imaging may provide timely tracing of leukocyte movement without disturbing the normal cellular or physiological status. With further investigation and validation by antibody labeling or cytometry assays, it is possible that such granularity traits of THG can assist in the lineage differentiation of leukocytes and have the potential to advance the study of research topics, such as the immune privilege of stem cells [22], or to capture tumor-immune or tumor-stromal cell interactions in metastatic microenvironments [23].

For clinical diagnosis, these granularity traits can help THG virtual optical biopsy [12–14] identify leukocytes in inflammation sites of skin or oral mucosa. To examine leukocytes in the interior of a hollow organ or cavity of the body, fiber-based THG endoscopy is required. Compared with other techniques, such as μ-OCT or spectrally-encoded microscopy, technical challenges for the implementation of endoscopy include miniaturized high-NA (NA > 0.8) focusing objectives, fibers with low nonlinearity, good THG collection efficiency with the same fiber, miniaturized scanning mechanism, and a compact laser system. In our preliminary studies, we have built a compact Cr:forsterite laser system [24], miniaturized the scanning system by a micro-electro-mechanical system mirror [25,26], used a multimode fiber to reduce pulse broadening [26], and successfully obtained sufficient THG signals through the same fiber [26]. Therefore, we believe THG endoscopy for the examination of leukocytes in the human body can be realized in the near future.

Acknowledgments

This study is funded by National Science Council Taiwan under the grant number NSC 100-2628-E-002-006 and by National Health Research Institutes under grant number NHRI-EX101-9936EI.

#171483 - $15.00 USD Received 27 Jun 2012; revised 6 Aug 2012; accepted 7 Aug 2012; published 24 Aug 2012